Vietnam Journal of Catalysis and Adsorption
Tạp chí xúc tác và hấp phụ Việt Nam

https://jca.edu.vn/

Study of physicochemical characteristics and layer-dependent deactivation behavior of industrial residue hydrodesulfurization (RHDS) catalysts

Huu Cuong Nguyen[1], Thi Thuy Le[1], Thi Hai Nam Chu[1], Anh Vu Nguyen[1], Hong Lien Nguyen[1,*]

[1] *School of Chemistry and Life Sciences, Hanoi University of Science and Technology, Viet Nam*
** Email: lien.nguyenhong@hust.edu.vn*

ARTICLE INFO

Received: 04/06/2026
Accepted: 27/06/2026
Published: 30/06/2026

Keywords:
RHDS; catalyst; physicochemical characterization

ABSTRACT

This study systematically examines the physicochemical characteristics and layer-dependent deactivation behavior of industrial residue hydrodesulfurization (RHDS) catalysts. A combination of EDS, XRD, BET, NH_3-TPD, and H_2-TPR analyses was employed to correlate elemental composition, structural characteristics, surface acidity, and reducibility. The results confirm that most of catalysts are based on alumina supports with highly dispersed active phases. Some catalyst layers exhibited enhanced acidity and a greater abundance of strong acid sites supporting for their different functions. Characterization of spent catalysts reveals significant deactivation caused by coke deposition and the accumulation of metal contaminants, particularly V and Fe, leading to pore blockage and structural alterations. These findings highlight the combined influence of acidity, reducibility, and catalyst-bed configuration on catalyst performance and deactivation, providing valuable guidance for improving RHDS catalyst efficiency and operational lifetime.

Introduction

Residue hydrodesulfurization (RHDS) units play a critical role in upgrading heavy petroleum residues containing sulfur-, nitrogen-, and metal-bearing compounds, as well as asphaltenes. These contaminants reduce product quality and accelerate catalyst deactivation through adsorption, pore blockage, and active-site poisoning. Their removal is achieved through catalytic hydrogenation reactions, including hydrodesulfurization (HDS), hydrodenitrogenation (HDN), hydrodemetallization (HDM), and aromatic hydrogenation.

Industrial RHDS reactors commonly employ multilayer catalyst beds with graded functionalities. The upper layers serve as guard and demetallization catalysts, while the lower layers provide enhanced hydrodesulfurization activity. This arrangement promotes the progressive removal of metals and coke precursors, thereby protecting the more active downstream catalysts. However, prolonged operation inevitably leads to catalyst deactivation caused by metal deposition, coke formation, and pore blockage along the reactor bed [1,2].

Sulfur removal proceeds through both direct desulfurization (DDS) and hydrogenation-mediated desulfurization (HYD), the latter being particularly important for refractory aromatic sulfur compounds. Simultaneously, HDN, HDM, aromatic hydrogenation, and limited hydrocracking reactions improve feed quality and reduce catalyst poisoning [1]. The RHDS unit investigated in this study comprises five sections: reaction, high-pressure hydrogen recycle, low-pressure separation, fractionation, and hydrogen make-up compression. The reaction section consists of two

https://doi.org/10.62239/jca.2026.02986

parallel trains, each containing three reactors in series, with two catalyst beds per reactor.

In this work, catalyst samples collected from different layers of the first reactor (R111) were characterized before and after service to evaluate structural, textural, acidic, and reducibility changes associated with catalyst deactivation. The results provide insight into layer-dependent deactivation behavior and the relationship between physicochemical properties and catalytic performance, contributing to the optimization of catalyst stacking and extension of catalyst service life.

Experimental

Catalyst samples

The catalyst bed configuration in Reactor R111 (shown in Figure 1) was designed with a multilayer structure to optimize the RHDS process while protecting the active catalyst zones from poisoning and flow maldistribution. The feed stream, consisting of hydrogen and hydrocarbon, enters from the top of the reactor and passes sequentially through several functional layers. At the top of the reactor, a void space combined with a distribution tray ensures uniform feed distribution and minimizes channeling effects before the reactants contact the catalyst bed. The first catalyst layer, Opti Trap MD (diameter of 16mm), plays a role as a filter for removal of impurities from the feed and protects the downstream catalyst layers from poisoning. The second protective layer consists of OptiTrap MR (diameter of 8.0 mm), which exhibits high thermal stability and effectively removes large contaminants from the feedstock, thereby reducing catalyst deactivation and promoting preliminary cracking reactions. This layer is followed by the OptiTrap Ring (diameter of 6.4 mm), which further improves flow distribution and traps residual particulate impurities. Beneath the guard layers, the RM-5030 (diameter of 5.6 mm) catalyst layer acts as a transition zone between the protective section and the main active catalyst bed, facilitating efficient dispersion of active phases and improving hydrodynamic stability. The primary reaction zone is composed of RM-8030 (diameter of 2.5 mm) and RM-8030S (diameter of 1.3 mm) catalyst layers, which are essential for hydrodesulfurization and other hydroprocessing reactions. The smaller particle size of RM-8030S increases the contact efficiency between reactants and catalytic active sites, thereby improving sulfur conversion performance. Another RM-8030 layer is subsequently placed below to maintain catalytic activity and reaction stability throughout the reactor bed.

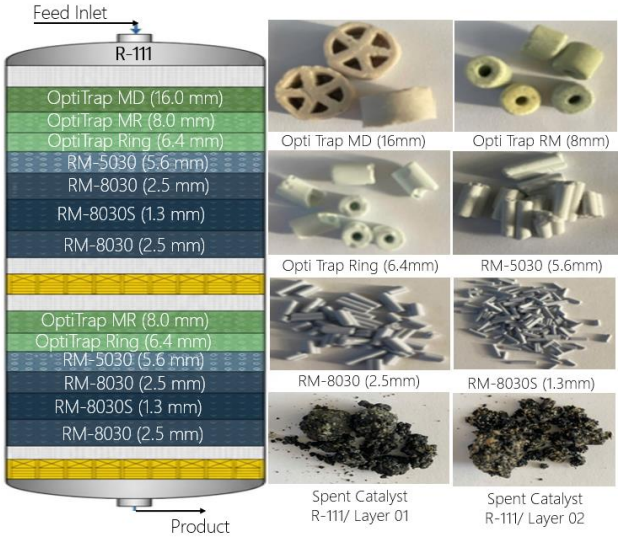

Reactor R111 – Catalyst Loading

Catalyst	Size (mm)	Function
OptiTrap MD	16	Filters impurities from the feed and protects the downstream catalyst layers from poisoning.
OptiTrap MR OptiTrap Ring	8.0 6.4	Exhibits high thermal stability, removes impurities, and promotes primary cracking reactions.
RM 5030 RM 8030 RM 8030S	5.6 2.5 1.3	A typical catalyst support in the RHDS process, providing a high surface area for effective dispersion of active phases.

Figure 1. The distribution of catalyst layers and their functions in the RHDS reactor (R111) [2] and Images of catalyst samples

These catalyst layers differ in both of morphology and color (Figure 1). While Opti Trap MD (16mm) is like beige wagon-wheels, Opti Trap MR (8 mm) appears as light cream rings and Opti Trap Ring (6.4 mm) is as pale grey-green cylinders. For the three active catalysts RM 5030, RM 8030, RM 8030S, they are all as bluish-grey cylinders, with finer for RM 8030S.

After approximately one year of operation, all catalysts in the three RHDS reactors of one train were unloaded for replacement with fresh one. During that period, two representative samples were collected from each bed of reactor R-111 and labeled as Spent Catalyst R-111_Layer 1, Spent Catalyst R-111_Layer 2. It should be noted that, due to catalyst withdrawal from the bottom section of the reactors and the inevitable mixing occurring during the unloading process, the collected catalyst samples were not exclusively represent the original individual layers, but rather consist of a mixture of catalysts from different layers in each bed.

https://doi.org/10.62239/jca.2026.029

Catalyst Characterization

The physicochemical properties of the catalyst samples were characterized using several complementary techniques. The crystalline structure was analyzed by X-ray diffraction (XRD) on a Bruker AXS D8 Advance diffractometer equipped with Cu Kα radiation (40 kV, 40 mA). Surface elemental compositions were determined by energy-dispersive X-ray spectroscopy (EDS) using a JEOL NeoScope JCM-7000 scanning electron microscope. Textural properties were evaluated from N_2 adsorption–desorption measurements performed at 77 K on a Micromeritics ASAP 2060. Prior to analysis, samples (0.2–0.5 g) were degassed at 200–300 °C, and the specific surface area was calculated using the Brunauer–Emmett–Teller (BET) method.

Catalyst reducibility and acidity were investigated by H_2 temperature-programmed reduction (H_2-TPR) and NH_3 temperature-programmed desorption (NH_3-TPD), respectively, using a Micromeritics AutoChem II 2920. Before each measurement, the samples were pretreated in He flow (30 mL min^{-1}) at 300 °C. For H_2-TPR, the reduction profiles were recorded from 50 to 900 °C under 10 vol.% H_2/Ar. For NH_3-TPD, the pretreated samples were cooled to 50 °C and saturated with 10 vol.% NH_3/He (30 mL min^{-1}) for 60 min, followed by helium purging for 60 min to remove physically adsorbed ammonia. The desorption profiles were then obtained by heating the samples to 900 °C.

Results and discussion

Morphology and elemental characterization

The EDS analysis results of all fresh and spent catalysts are summarized in Table 1.

Table 1. EDS characterization of catalyst samples

Sample	% Weight										
	O	Al	Si	Mo	Ni	Co	P	C	V	S	Fe
Opti Trap MD	58.6	11.78	25.31	-	-	-	-	-	-	-	
Opti Trap MR	53.79	41.31	2.01	2.49	0.39	-	-	-	-	-	
Opti Trap Ring	52.99	37.7	0.73	7.33	1.26	-	0.49	-	-	-	
RM 5030	52.8	41.43	-	4.82	0.67	-	0.68	-	-	-	
RM 8030	55.93	37.97	0.31	4.59	0.41	0.48	0.31	-	-	-	
RM 8030S	55.03	37.74	0.5	5.5	0.37	0.52	0.34	-	-	-	
R111 -Layer 1	42.8	13.2	-	-	1.75	-	-	29.4	5.6	7	0.2
R111 -Layer 2	38.1	12.6	0.2	-	0.8	-	-	36.4	3.6	5.9	1.7

As shown in Table 1, the OptiTrap MD sample contains only O, Al, and Si, with Si/Al ratio of 2.15. Based on the EDS analysis, this Si/Al ratio allows two possible interpretations. First, the support may contain zeolite Y, since the obtained ratio falls within the typical range reported for zeolite Y (Si/Al = 2–5). Alternatively, the support may consist of mixed Al_2O_3 and SiO_2 phases formed through the combination of these two oxides. Therefore, the Si/Al ratio alone is insufficient to unambiguously identify the support structure, and additional characterization is required to distinguish between these possibilities.

The OptiTrap MR sample is dominated by O (53.79 wt.%) and Al (41.31 wt.%), indicating an alumina-based support with negligible zeolitic character due to its low Si content (2.01 wt.%). The presence of Mo (2.49 wt.%) and Ni (0.39 wt.%) confirms a dispersed Ni–Mo active phase on Al_2O_3. This composition is characteristic of demetallization catalysts employed in the upper section of RHDS reactors to capture metals and other contaminants from the feedstock, thereby preserving the activity of downstream catalysts.

The OptiTrap Ring, RM 5030, RM 8030 and RM 8030S samples are also primarily composed of oxygen and aluminum, indicating γ-Al_2O_3-based supports with very low silicon contents (≤0.73 wt.%). Active metals including Mo, Ni, and Co are dispersed on the support with concentrations varying according to catalyst function. The OptiTrap Ring and RM 5030 catalysts contain more Mo and Ni, consistent with their roles as transition or guard layers. In contrast, RM 8030 and 8030S contain Co in addition to Mo and Ni, characteristic of Co–Mo/Ni–Mo hydroprocessing catalysts. Furthermore, the presence of phosphorus (0.31–0.68 wt.%) in all four types of catalysts OptiTrap Ring, RM 5030, RM 8030 and RM 8030S indicates its role as a promoter, improving active-metal dispersion and catalyst stability.

https://doi.org/10.62239/jca.2026.029

For the spent catalysts, EDS analysis revealed the appearance of additional elements, including C, V, S and Fe, in both R111 Layer 1 and R111 Layer 2 compared with the fresh catalysts. The detection of carbon and sulfur indicates the deposition of coke and sulfur-containing species, while the accumulation of Fe and V reflects contamination from the heavy feedstock. These deposits are known to block catalyst pores, cover active sites, and accelerate catalyst deactivation during long-term RHDS operation. The elemental composition of the different materials is suited to the distribution of the catalytic layers and their functions in the RHDS reactor (R111).

Crystalline phase characterization

Figure 2 shows the XRD patterns of the fresh and spent catalysts. As shown in Figure 2a, the XRD pattern of the OptiTrap MD sample is dominated by diffraction peaks characteristic of quartz low ($2\theta \sim 26.6°$, with the most prominent characteristic d-spacings recorded as d = 4.247 Å, d = 3.335 Å), alongside prominent Mullite reflections such as d = 5.371 Å, d = 3.416 Å, and d = 2.689 Å. The XRD pattern of the OptiTrap MD sample exhibits a biphasic structure comprising a chemically inert Quartz matrix (~71%) intertwined with highly thermo-mechanically resilient Mullite crystals (~20%). In contrast, the characteristic reflections of zeolite Y ($2\theta \approx$ 10.3°, 12.2°, 16.0°, 19.1°, 20.7°, 23.3°, 24.1°, and 27.6°) are absent, indicating that no zeolitic phase is present in this catalyst. The predominance of SiO2 suggests a thermally stable structure with high mechanical strength, which is desirable for guard catalysts operating under severe hydrotreating conditions [3, 4]. Combined with the EDS results, the catalyst can be identified as an α-Al_2O_3–SiO_2-based material designed for impurity trapping and protection of downstream catalyst layers.

The diffraction pattern of OptiTrap MR reveals reflections attributable to MoO_3, consistent with the presence of Mo detected by EDS analysis and in agreement with previous reports. Additional reflections associated with NiO/NiO_x and α-Al_2O_3 were also observed [5], indicating that active Ni and Mo species are dispersed on an alumina support. The incorporation of SiO_2 is expected to enhance thermal stability and mechanical resistance, supporting the catalyst's role in impurity removal and preliminary cracking reactions before the feed reaches the main hydroprocessing catalysts.

The remaining fresh catalysts exhibit similar XRD patterns, characterized by the typical γ-Al_2O_3 reflections at approximately 37.5°, 45.9°, and 66.8° (Figure 2b). γ-Al_2O_3 is widely employed in hydrotreating catalysts because of its high surface area and excellent ability to disperse active metal species [6]. No distinct diffraction peaks corresponding to active phases were detected, suggesting that Mo-, Ni-, and Co-containing species are highly dispersed and/or present as very small crystallites (<4 nm), consistent with previous studies on supported hydroprocessing catalysts [7].

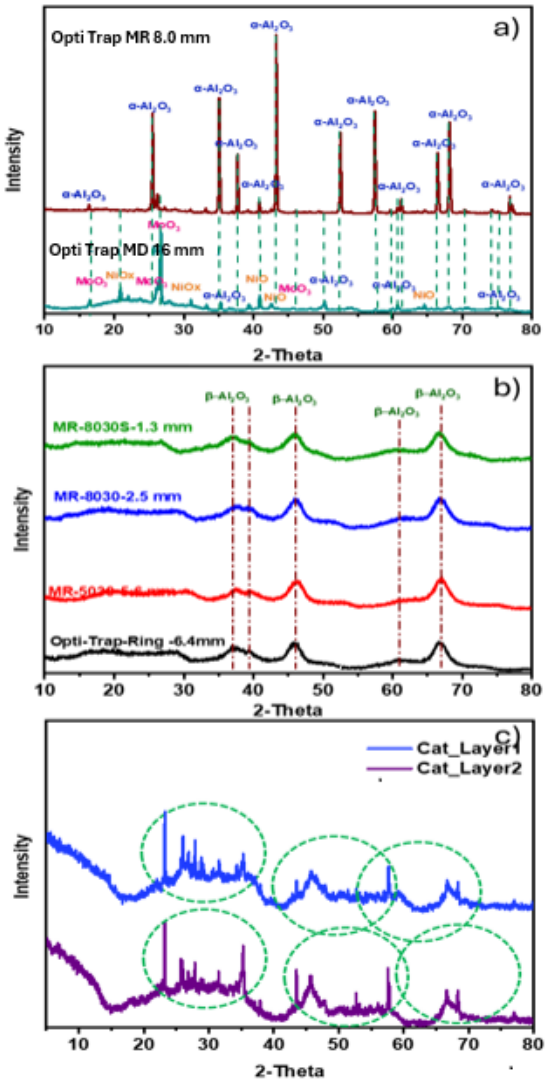

Figure 2. XRD patern of fresh (a, b) and spent (c) catalysts

For the spent catalysts, several additional diffraction peaks appeared on the γ-Al_2O_3 background, indicating the formation of new crystalline phases during operation. Together with the EDS results, which revealed the accumulation of C, S, Fe, and V, these observations provide strong evidence of catalyst deactivation caused by coke deposition and metal poisoning. The newly emerged reflections in the 2θ ranges of 25–35°, 45–60°, and 65–70° can be tentatively assigned to iron sulfide phases, including FeS, Fe_7S_8, and FeS_2, as well as vanadium sulfides such as VS_2, VS_4, and V_2S_3. However, significant overlap among the diffraction peaks prevents the unambiguous identification of individual phases.

https://doi.org/10.62239/jca.2026.029

The formation and accumulation of Fe and V sulfides, together with coke deposits, progressively cover the active Mo-, Ni-, and Co-based sites, resulting in a loss of catalytic activity. In addition, these deposits tend to accumulate near pore entrances, causing pore blockage and restricting the diffusion of reactants and products within the catalyst particles. Consequently, mass-transfer limitations become more pronounced, accelerating catalyst deactivation and reducing overall hydroprocessing performance

Specific surface area and porous structure

BET surface area and pore size distribution of catalyst samples were presented in Figure 3.

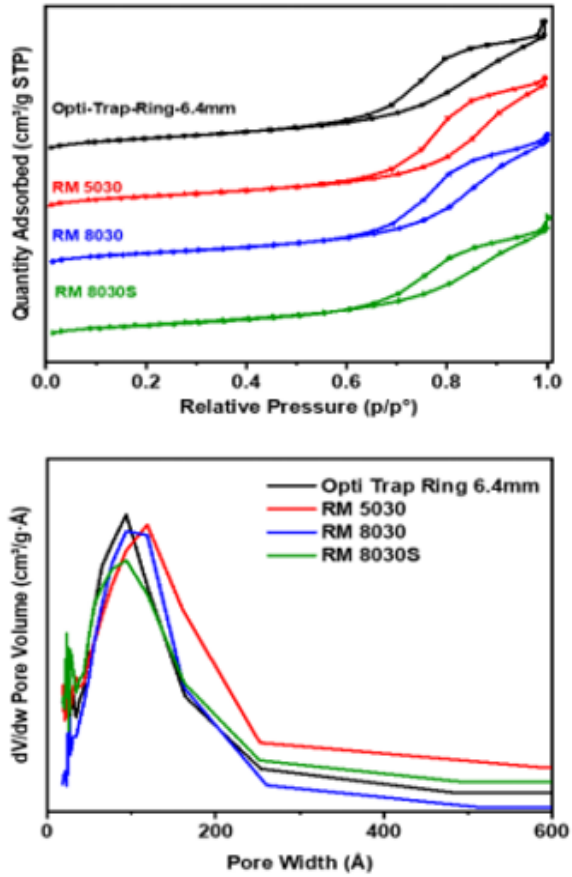

Sample	Surface area (m^2/g)	Pore Volume (cm^3/g)	Pore size (Å)
Opti Trap Ring	258.15	0.59	98.12
RM 5030	242.68	0.63	111.71
RM 8030	243.37	0.64	108.33
RM 8030S	236.69	0.56	97.41
R111-Layer 1	27.81	0.06	118.12
R111-Layer 2	25.76	0.04	162.94

Figure 3. N_2 adsorption–desorption isotherms, pore size distribution and BET surface area of catalyst samples.

As can be observed from the Figure 3, fresh catalyst samples exhibit type IV isotherms with H1 hysteresis loops, confirming mesoporous structures according to IUPAC classification. The similar H1 loops suggest nearly spherical particles with cylindrical pores or aggregates of spherical particles. This also indicates that the active phases are finely dispersed within the γ-Al_2O_3 pores without significantly altering the pore structure. The pore size distribution (Figure 3b) reveals two main regions centered at ~100 Å and below 50 Å. Compared with typical γ-Al_2O_3 (pore size 60 - 120 Å), this distribution suggests the influence of binders used during commercial granulation, and the presence of SiO_2 is consistent with EDS results.

The Opti-Trap-Ring 6.4 mm sample shows the highest surface area (~258 m^2/g) and narrow pore distribution, favoring dispersion of active phases and enhancing downstream HDS and HDN reactions [8]. Meanwhile, RM 5030 5.6 mm, with large pore size and high pore volume, is suitable for HDM and early removal of Ni and V. The rest RM 8030 2.5 mm and RM 8030S 1.3 mm samples, with moderate pore sizes and high surface areas, mainly promote sulfur removal and completion of HDS reactions.

In contrast to the fresh catalyst samples, both of the spent catalysts R-111 Layer 1 and R-111 Layer 2 exhibited a drastic reduction in specific surface area (26-28 m^2/g), dropping by approximately tenfold compared to the fresh counterparts, accompanied by a notable increase in the average pore diameter (from 97–111 Å to 118–162 Å). This inverse correlation strongly indicates that the deactivation mechanism is predominantly governed by selective pore blockage rather than structural collapse of the γ-Al_2O_3 support.

Acidity characterization

The TPD-NH_3 profile provide clear quantitative and qualitative evidence of surface acidity of RM 8030S as shown in Figure 4.

As can be observed from the Figure 4, the RM 8030S sample showed dominant NH_3 desorption peaks at low temperatures (~104 °C), corresponding to weak acid sites. However, it also exhibited pronounced desorption characteristics in the mid- and high temperature regions (378.7–771.5 °C), confirming the presence of high proportion of medium and strong acid sites. The total acidity of this catalyst was 0.507 mmol NH_3/g. Overall, the high acidity and strong acid site distribution of RM 8030S are expected to significantly affect its catalytic performance, especially in acid strength-sensitive reactions [9].

https://doi.org/10.62239/jca.2026.029

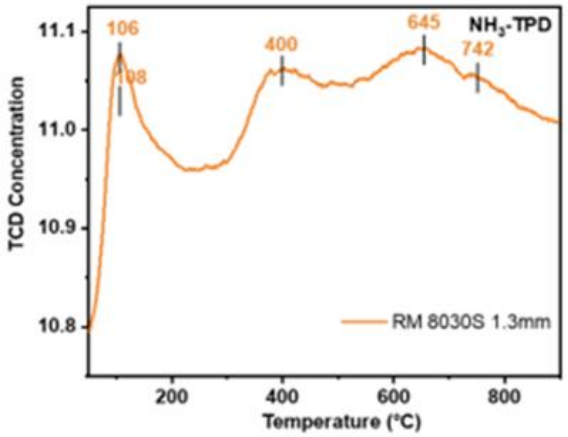

Temperature (°C)	NH_3 (mmol/g)	Total NH_3 (mmol/g)
104.5	0.33	
378.7	0.11	
660.5	$5.7.10^{-2}$	0.507
771.5	$1.0.10^{-2}$	

Figure 4. TPD-NH_3 profile of RM 8030S

Reducibility of components in catalysts

The H_2-TPR results further clarify the effect of metal composition on the reducibility of the catalysts. As can be seen in Figure 5, the RM 8030S (1.3 mm) shows reduction peaks at high temperatures (420 and 700 °C), reflecting the presence of Co species, which are difficult to reduce.

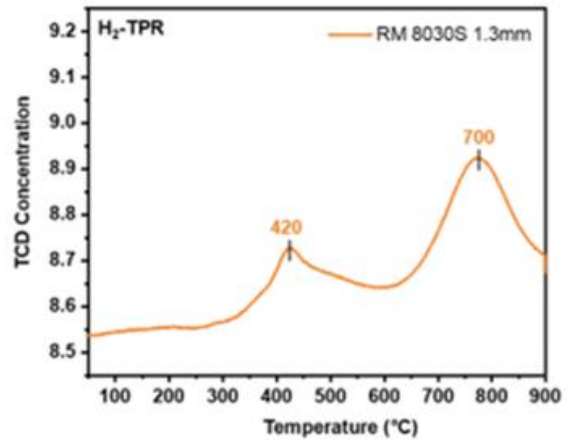

Temperature (°C)	H_2 (mmol/g)	Total H_2 (mmol/g)
420	0.22	0.69
700	0.47	

Figure 5. TPR-H_2 profile of RM 8030S

This suggests stronger metal–support interactions and lower reducibility. These observations are consistent with the XRD and EDS analyses, confirming the role of metal dispersion and composition in governing the redox behavior of the catalysts [10].

Conclusion

This study comprehensively evaluated the physicochemical properties and layer-dependent deactivation behavior of industrial residue hydrodesulfurization (RHDS) catalysts before and after service. Based on the experimental findings, several key conclusions can be drawn. For the fresh samples, most of the investigated catalysts are based on γ-Al_2O_3 supports with highly dispersed active phases (Mo, Ni, Co) and phosphorus (P) as a promoter. In contrast, the top guard layer possesses a thermo-mechanically resilient biphasic structure consisting of Quartz and Mullite within an α-Al_2O_3–SiO_2 matrix, optimized for mechanical filtering and impurity trapping. All active catalysts exhibit mesoporous structures with a bimodal pore-size distribution. NH_3-TPD and H_2-TPR analyses, specifically exemplified by the RM 8030S sample, elucidated a strong correlation between surface acidity, redox behavior with the role of catalyst in the processes of hydrodesulfurization. For the spent catalysts, a drastic tenfold reduction in specific surface area alongside a notable increase in the average pore diameter, the accumulation of heavy metal contaminants (V and Fe as crystalline sulfide phases) confirmed that deactivation is primarily driven by coke deposition, causing selective pore blockage and active-site coverage. This research supplies preliminary results for further research on optimizing catalyst selection and bed configuration to enhance catalytic efficiency of industrial RHDS units.

References

1. S.Y. Ahn, W.J. Na, K.J. Kim, B.J. Kim, H.K. Park, H.S. Roh, Catalysts, 13(4) (2023) 738. https://doi.org/10.3390/catal13040738
2. A.K. Rhodes, Oil Gas J., 92(22) (1994) 64-74.
3. J.M. Amigó, F.J. Serrano, M.A. Kojdecki, J. Bastida, V. Esteve, M.M. Reventós, F. Martí, J. Eur. Ceram. Soc., 25(9) (2005) 1479-1486. https://doi.org/10.1016/j.jeurceramsoc.2004.05.019
4. R.S. Suharbiansah, M.F. Lukman, C. Nannuzzi, A. Wach, K. Góra-Marek, M. Liebau, M. Jabłońska, Catal. Sci. Technol., 13(13) (2023) 3804-3817. https://doi.org/10.1039/D3CY00269A
5. H. Yan, D. Zhang, J. Xu, Y. Lu, Y. Liu, K. Qiu, Y. Luo, Nanoscale Res. Lett., 9(1) (2014) 424. https://doi.org/10.1186/1556-276X-9-424
6. F. Saira, N. Firdous, R. Qureshi, A. Ihsan, Turk. J. Chem., 44(2) (2020) 448-460. https://doi.org/10.3906/kim-1910-21
7. H. Li, J. Li, Y. Han, X. Chen, C. Fan, G. Liu, X. Wang, Carbon Resour. Convers., (2026) 100418. https://doi.org/10.1016/j.crcon.2026.100418
8. A. Stanislaus, A. Marafi, M.S. Rana, Catal. Today, 153(1-2) (2010) 1-68. https://doi.org/10.1016/j.cattod.2010.05.011
9. S. Beshkoofeh, B. Ghalami-Choobar, Z. Shahidian, S. Khosharay, Iran. J. Chem. Chem. Eng., 40(6) (2021) 1777-1792. https://doi.org/10.30492/ijcce.2020.127829.4161
10. S.Y. Ahn, W.J. Na, K.J. Kim, B.J. Kim, S.J. Ryu, H.S. Roh, H.K. Park, Catal. Today, 425 (2024) 114335. https://doi.org/10.1016/j.cattod.2023.114335